

High Resolution Helioseismic Imaging of Subsurface Structures and Flows of A Solar Active Region Observed by Hinode

Junwei Zhao, Alexander G. Kosovichev

W. W. Hansen Experimental Physics Laboratory, Stanford University, Stanford, CA94305-4085

and

Takashi Sekii

National Astronomical Observatory of Japan, 2-21-1 Osawa, Mitaka, Tokyo 181-8588, Japan

ABSTRACT

We analyze a solar active region observed by the *Hinode* Ca II H line using the time-distance helioseismology technique, and infer wave-speed perturbation structures and flow fields beneath the active region with a high spatial resolution. The general subsurface wave-speed structure is similar to the previous results obtained from *SOHO*/MDI observations. The general subsurface flow structure is also similar, and the downward flows beneath the sunspot and the mass circulations around the sunspot are clearly resolved. Below the sunspot, some organized divergent flow cells are observed, and these structures may indicate the existence of mesoscale convective motions. Near the light bridge inside the sunspot, hotter plasma is found beneath, and flows divergent from this area are observed. The *Hinode* data also allow us to investigate potential uncertainties caused by the use of phase-speed filter for short travel distances. Comparing the measurements with and without the phase-speed filtering, we find out that inside the sunspot, mean acoustic travel times are in basic agreement, but the values are underestimated by a factor of 20 – 40% inside the sunspot umbra for measurements with the filtering. The initial acoustic tomography results from *Hinode* show a great potential of using high-resolution observations for probing the internal structure and dynamics of sunspots.

Subject headings: Sun: helioseismology — Sun: sunspots — Sun: interior

1. Introduction

Deriving subsurface structures and flow fields of solar active regions is one of the major topics for local helioseismology studies. Using Ca II K observations made at the geographic

South Pole in early 1990s, Duvall et al. (1996) found the first evidence of downdrafts below active regions through measuring acoustic travel times by employing the time-distance helioseismology technique. Later inversions (Kosovichev 1996) using these travel time measurements found strong converging downflows and areas of the excess of sound-speed beneath growing active regions. With the availability of *Solar and Heliospheric Observatory* / Michelson Doppler Imager (*SOHO/MDI*; Scherrer et al. 1995) Doppler observations that are seeing-free and more suitable for local helioseismology studies, more investigations of the sunspot's subsurface structures and flow fields have been carried out by use of various theoretical models: ray-path approximation (e.g., Kosovichev et al. 2000; Zhao et al. 2001), Fresnel-zone approximation (e.g., Jensen et al. 2001; Couvidat et al. 2004), and Born approximation (e.g., Couvidat et al. 2006). Despite the use of different approaches of calculating travel time sensitivity kernels, the results remain largely the same, i.e., for active region subsurface structures, a negative sound-speed perturbation was found up to 5 Mm below the photosphere, and a positive perturbation was seen below that depth. For subsurface flow fields, converging downflows were inferred from the photosphere to about 5 Mm beneath it, and divergent flows were found below this layer. Another local helioseismology technique, ring-diagram analysis, although could not provide subsurface flow maps with such a high spatial resolution, gave results that were in general agreement (Haber et al. 2004; Komm et al. 2005). Some direct comparisons of these two techniques were also performed (Hindman et al. 2004).

However, on the other hand, these results were not uncontroversial. By measuring acoustic phase shifts in sunspot penumbra using MDI Doppler observations when sunspots were located near the solar disk limb, Schunker et al. (2005) demonstrated that the measured acoustic travel times varied around sunspot penumbra when the sunspot was located near the limb, and believed this effect was caused by the inclined magnetic field. While acknowledging the existence of such an effect in oscillation signals observed in Dopplergrams, Zhao & Kosovichev (2006) found out that such an effect did not exist in the oscillations observed in MDI continuum intensity. Additionally, Rajaguru et al. (2006) showed that the phase-speed filtering in the time-distance acoustic travel time measurements would also introduce errors in active regions where oscillation amplitudes were suppressed. Using numerical simulations Parchevsky et al. (2008) confirmed this effect, and concluded that this effect led to underestimation of the mean travel times at short distances. Some recent attempts of using different filtering procedures, e.g., ridge filtering (Braun & Birch 2008), showed that different filtering might give different measurements. Thus, it is certainly worthwhile examining how filters would change measurement results. On the other hand, it is also arguable whether those time-distance observed acoustic travel time variations in solar magnetic areas could be interpreted as interior sound speed anomalies, or were caused by some surface magnetism effects such as showerglass effect (Lindsey & Braun 2005a,b). Furthermore, it is also not clear how the interaction of acoustic waves and magnetic field would effect the phase of these waves, hence the travel time variations in the measured acoustic travel times. It would be very difficult

to interpret the measurements if acoustic waves experience some phase shifts at the boundary of unmagnetized and magnetized areas (Cally 2009).

High spatial resolution observation of sunspots by the Solar Optical Telescope (SOT; Tsuneta et al. 2008) onboard the Japanese solar spacecraft *Hinode* (Kosugi et al. 2007) not only gives us another possibility of investigating subsurface properties of solar active regions in addition to the already existing helioseismology instruments, but also provides an unprecedented high spatial resolution that has enabled some studies that were improbable using these existing instruments. In this paper, we analyze an active region observed by *Hinode* utilizing the time-distance helioseismology technique, and infer the wave-speed profiles and flow fields beneath this region, and present these results in §3. We also analyze the acoustic signals without applying any filters except filtering out solar convection and f -modes, and investigate how the phase-speed filtering effects our measurements. Such analyses can hardly be carried out by use of MDI high resolution observations, and these results are presented in §4. In §5, we discuss and summarize our results.

2. Observation and Data Analysis

The sunspot inside active region NOAA AR10953 was observed by *Hinode*/SOT Ca II H line continuously for a total of 738 minutes, from 17:00UT May 2 through 05:58UT May 3, 2007, with a cadence of approximately 1 min. The cadence was not uniform, but had a variation of a fraction of 1 sec, and this was corrected by interpolating data into a uniform time grid of 1 min. Each image, 2048×1024 pixels in size, has a spatial resolution of $0.108''/\text{pixel}$, and a field of view of approximately 160×80 Mm. An image from this observation is shown in Figure 1. We perform a 2×2 rebin before time-distance analysis, and the resultant resolution is corresponding to 0.156 Mm/pixel. During this 12+ hours observation, the pointing of SOT was not sufficiently stable, and this is corrected by shifting images to keep the sunspot center in a fixed location during the whole sequence.

As demonstrated by Sekii et al. (2007) and Nagashima et al. (2009), the time-distance helioseismology technique works well with the *Hinode* Ca II H data. We apply the similar measurement and inversion procedure on this active region. Seven different time-distance measurement annuli are used, and the annulus ranges are 4.0 – 6.6, 6.5 – 9.7, 9.2 – 12.5, 12.0 – 15.9, 15.1 – 18.9, 18.5 – 22.3, and 21.6 – 25.4 Mm, respectively. Because of the limited field of view, longer annuli cannot be used in measuring this dataset, and this restricts us from reaching deeper interiors. When we fit the cross-covariance inside the sunspot umbra and penumbra some misfittings occur, but the number of misfittings is insignificant, and this should not alter our analysis and final results. The misfitted pixels are replaced by averaged values from their neighboring pixels.

After the acoustic travel times are measured, inversions are performed to infer the subsurface magnetoacoustic wave-speed structures and flow fields. The inversion technique, sensitivity kernels, and the final averaging kernels are essentially the same as or similar to those presented by Zhao et al. (2007) except the slightly different annulus radii and depth coverage.

3. Subsurface Structure and Flow Field

3.1. Subsurface Wave-Speed Structure

A few selected images of the inverted wave-speed perturbations at different depths are displayed in Figure 2. At depths shallower than ~ 3 Mm, the wave-speed perturbation is dominantly negative inside the sunspot area, although small areas of positive perturbations exist, in particular, close to a light bridge in the upper umbra area. At the depth of 3.0 – 4.5 Mm, negative and positive wave-speed perturbations are mixed. Below approximately 6 Mm, the perturbations are predominantly positive inside the sunspot area. Please note that all depths here are relative to where the Ca II H line forms and the acoustic signals are observed, i.e., approximately 250 km above the solar photosphere (Carlsson et al. 2007).

A vertical cut through the center of the sunspot along the East-West direction at $Y = 39$ Mm, as presented in Figure 3, shows that the wave-speed anomalies extend about half of the sunspot size beyond the sunspot penumbra horizontally. In the vertical direction, the negative wave-speed perturbation extends to a depth of ~ 4 Mm. The positive perturbation is about 9 Mm deep, but it is not clear whether it extends further, because our inversion cannot reach deeper layers due to the limited field of view. The averaging kernels associated with this inversion are shown in Figure 4.

In the quiet Sun, the measured mean acoustic travel times often appear to be relatively constant with little correlation with supergranulation structures. Hence we can estimate our travel time measurement uncertainties by computing standard deviations in a region of the quiet Sun. The errors in the inverted wave speed structures can then be estimated by convolving the measurement uncertainties with the averaging kernels. These error estimates are shown in Figure 5. It is found that the errors decrease and the averaging kernels become broader with the increase of depth. This is a general property of helioseismic inversions, and the error magnitude and averaging kernel width depend on the choice of regularization parameters. In this case, the parameters are chosen to provide a sufficient smoothing of the regularized solution at different depths. This results in broader averaging kernels and smaller error estimates in deeper layers.

This picture of sunspot’s subsurface wave-speed perturbation is made from intensity observations, rather than more commonly used Doppler velocity data. In spite of this, the subsurface wave-speed structure is remarkably similar to the previous results obtained using MDI Dopplergrams

and various types of the acoustic sensitivity kernels (e.g., Kosovichev et al. 2000; Couvidat et al. 2006; Zharkov et al. 2007). It is also noticeable that no obvious effect caused by the inclined magnetic field is visible in the inverted sound speed perturbation map, although the sunspot is located quite a distance away from the solar disk center. This is in agreement with the conclusion of that the solar oscillation signals observed in intensity are not affected by inclined magnetic fields (Zhao & Kosovichev 2006). Unfortunately, a direct comparison with MDI is not possible because of the lack of simultaneous uninterrupted observations for this sunspots or other sunspots.

3.2. Subsurface Flow Field

A few selected three-dimensional velocity maps are displayed in Figure 6 after a 4×4 re-binning in horizontal velocities in order to reveal more clearly the larger-scale patterns. It can be found that at the depth of 0 to 3 Mm, the plasma flows towards the boundary of sunspot penumbra from outside. Inside the sunspot penumbra, the horizontal flow fields are not clearly organized in the rebinned images, but look well organized in the original high resolution flow maps (see §3.3). Beneath 3 Mm, the horizontal flow field is largely divergent from the sunspot area, and extends quite far away. The vertical flows are directed mostly downward until at least 4.5 Mm in depth inside the sunspot area. Below 6 Mm or so, there seems to be a mixture of the downward and upward flows in this region.

A vertical view of the flow field (Figure 7) after linear interpolation shows nicely the flow structure beneath the active region. Strong downdrafts are seen immediately below the sunspot's surface, and extends up to 6 Mm into the deep. The downdraft has a maximum speed larger than 500 m/s, and is much stronger than the vertical flow speed expected in supergranular structures. A little beyond the sunspot's boundary, one can find both upward and inward flows. Clearly, large-scale mass circulations form outside the sunspot, bringing plasma down along the sunspot's boundary, and back to the photosphere within about twice of the sunspot's radius. It is remarkable that such an apparent mass circulation is obtained directly from the helioseismic inversions without applying any additional inversion constraints, such as forced mass conservation. The mass circulation pattern in the previous MDI results (Zhao et al. 2001) was not that clear.

Based on analysis of artificial data, Zhao & Kosovichev (2003) demonstrated that a divergent (convergent) flow structure would result in a downward (upward) vertical flow due to cross-talk effect, making the inversion of small vertical speed difficult or even impossible by our inversion technique. The same effect was also discussed by Zhao et al. (2007) to explain why they could not invert vertical flows from the numerical simulations of the quiet Sun. However, the downward flows found in this study is not due to the cross-talk effect, because the inflows around active region found in this study would have caused upward speed due to this effect. This means that

in our results the inferred downward flows are probably underestimated although it is not clear by how much. At the moment, we do not know how to offset this effect in our inversions. This requires more work with sunspot numerical simulation data. However, it is important to emphasize that this effect does not affect the qualitative picture of the flow pattern below the sunspot obtained in our inversions.

3.3. High Resolution Subsurface Flow Field

Due to the very high spatial resolution of *Hinode* observation, the time-distance analysis can also give high resolution flow fields. One example, the horizontal flow field at 0 – 1.5 Mm beneath the sunspot area, is shown in Figure 8. From this flow map, one can easily identify small-scale divergent flow structures inside both the sunspot umbra and penumbra. The scale of these flow structures, 4 – 5 Mm, is larger than the typical scale of solar granulations (1 – 2 Mm), but smaller than supergranulations (20 – 30 Mm). The speed of these flows is about 300 – 500 m/s. They probably represent convective cells in subsurface magnetized plasma of sunspots. It is intriguing that small-scale vortex motions below sunspots were suggested by Parker (1992) as a key element of the cluster sunspot model.

However, one should also be cautious in interpreting these small-scale structures. The scale of these structures is similar to the wavelength of acoustic waves used for the inferences at this depth, approximately 3 Mm. At this point, it is not clear how well the structures of this scale are resolved in our measurements. But the evidence of small-scale structures below sunspots is quite interesting, and certainly requires more observational and modeling studies.

Another remarkable phenomenon in this high resolution flow map is that in the light bridge area, located inside the upper part of the sunspot umbra (at $X = 28\text{--}32$ Mm and $Y = 33\text{--}37$ Mm), the flows are divergent from the bridge with a speed of ~ 400 m/s. This shows a strong coupling between the sunspot structure and subsurface dynamics. Thus, the high resolution subsurface flow can be useful to monitor the dynamics and evolution of sunspots.

4. Analysis without Phase-Speed Filtering

4.1. Averaged Travel Times

It has long been recognized from analysis of *SOHO*/MDI data that for short distances, the time-distance cross-covariance functions from measurements may be corrupted by some signals that are not well understood (Duvall et al. 1997). In Figure 7, we compare the time-distance di-

agrams calculated for the *Hinode* observing run and for high-resolution MDI data of the same duration and the same area size. As shown in the left panel of Figure 9, for the high resolution MDI observations, when the distance is smaller than ~ 8 Mm, the acoustic wave propagation signal is essentially lost in some horizontal stripes, which block the measuring of acoustic travel times in this distance range. It is not yet well understood how these horizontal stripes are generated, but they are thought to be related to the instrument modulation transfer function (MTF) and instrumental distortions. Phase-speed filtering was introduced to reduce the influence of these horizontal stripe signals at short distances (Duvall et al. 1997), but prior to the *Hinode* data there is yet no way to investigate the effectiveness and accuracy of this procedure.

With the availability of *Hinode* high resolution helioseismology observations, this difficulty can be resolved or partly resolved. In the *Hinode* time-distance diagram shown in the right panel of Figure 9, the acoustic signals are very nicely visible in very short distances as small as ~ 2 Mm, although some shorter and weaker horizontal stripes still exist. Judging from this time-distance diagram averaged from the observations in the whole field of view as displayed in Figure 1, it should be possible to make the travel time measurements for travel distances shorter than 4 Mm even without using the phase-speed filter.

Without using the phase-speed filter (but with f -modes and solar convection filtered out), we obtain three different time-distance diagrams when the central points of the annulus are located inside a quiet solar region, sunspot penumbra, and sunspot umbra, respectively. These time-distance diagrams are obtained after averaging the outgoing and ingoing, i.e., both positive and negative lags of, cross-covariance functions. For a better comparison the quiet solar region is chosen a size similar to the sunspot umbra. The Gabor wavelet fitting (Kosovichev & Duvall 1996) is used to infer the acoustic travel times for different distances and for all three diagrams, and the results are shown in Figure 10. The time-distance diagram looks quite noisy for the sunspot umbra, and less noisier for the sunspot penumbra. However, the acoustic wave propagation signals are strong and clear in both cases, and a robust fitting is not a problem for both diagrams.

It can be found that the measured acoustic travel times are longer than the ray theory expectations at distance of about 6 – 7 Mm. This may be due to that the second-skip signals are not completely separated from the first-skip signals, and the fitted values are thus slightly elevated. Since the travel time measurements inside the sunspot and in the quiet Sun should be similarly affected in the fitting, it is useful to use the quiet Sun measurements as a reference at this distance. To better understand the travel time anomalies inside sunspots, we use the travel time measured in the quiet Sun as a reference, and study the relative travel times after the reference is subtracted from the travel times measured in the sunspot umbra and penumbra (see Figure 11a and 11b). It is clear that acoustic travel times measured inside the sunspot umbra and penumbra are quite similar, and both exhibit a positive anomaly of ~ 40 sec when the distance is smaller than approximately

12 Mm, and a negative anomaly of ~ 35 sec when the distance is between approximately 14 and 21 Mm.

For the correct interpretation of the travel time measurements, it is extremely interesting to compare these measurements with and without the phase-speed filter. For the measurements with the phase-speed filtering, we average the mean travel times, which are measured by use of 7 different annulus ranges using different phase-speed parameters as presented in §3, inside the sunspot umbra and penumbra separately. Figures 11c and 11d display such a comparison. It can be found that for both sunspot umbra and penumbra, the measurements with and without the phase-speed filtering are quite similar, i.e., the travel time anomalies are positive for travel distances shorter than ~ 13 Mm, but become negative for larger distances. However, it appears that for the sunspot umbra, the measurements with the phase-speed filtering underestimate the values by a factor of 20 – 40%; and for the sunspot penumbra, the values are also underestimated, but by a smaller factor. This underestimation is expected due to a combination of the smaller oscillation amplitude in active regions and the use of phase-speed filtering (Rajaguru et al. 2006; Parchevsky et al. 2008).

4.2. Travel Time Map

We have compared the averaged one-dimensional mean travel time curves with and without the phase-speed filtering, and it is interesting to compare two-dimensional acoustic travel time maps that are obtained from two sets of different measurements. As it is well known that travel time measurements without filtering are noisier, we have succeeded in making clean travel time maps for only three annuli among the seven that are presented in §3. Figure 12 shows one such example of comparing mean travel time maps with and without the filtering. There are many similarities as well as discrepancies between these two travel time maps. It is clear that at this measurement distance, for both measurements, the negative travel time anomalies are found outside the sunspot area, and mixed positive and negative time anomalies exist inside the sunspot. However, it is also clear the detailed structure of the map look different. Such comparisons are still at an early stage, and we believe a systematical study over such comparisons would lead us to a better understanding how phase-speed filtering, as well as other filtering practices, effect measurements. Obviously, longer time series of high-resolution sunspot observations will help to improve the results.

5. Discussions and Summary

5.1. Subsurface Structure and Flow Field

By a time-distance analysis of unprecedented high spatial resolution observations from the *Hinode*/SOT, we have investigated high resolution wave-speed structures and mass flows beneath active region AR10953. For the subsurface wave-speed structure, the inverted results are remarkably similar to previous results based on MDI Dopplergrams with different inversion technique as well as different sensitivity kernels. For subsurface flow fields, the general picture is similar to what has been obtained from MDI observations, i.e., converging downward flows near the surface below the sunspot area. Despite the similarities, the current picture also has some differences compared with the earlier one. One difference is that the downward flows beneath the sunspot are more prominent in the flow fields inferred from this study. Another remarkable result from this study is the mass circulation outside the sunspot, which seems to keep mass conservative and is much more clear than the previous MDI inversions. It is widely believed in theory and in numerical simulations that such downdraft and converging flows near the sunspot surface play important roles in keeping sunspots stable (Parker 1979; Hurlburt & Rucklidge 2000; Hurlburt & DeRosa 2008).

However, it is still not quite clear how the overall flow structures around the sunspot's surface and interior look like. It is already well known the existence of penumbral Evershed outflows, outgoing moat flows beyond sunspot's penumbra, and inflows from the inner penumbra and umbra measured by tracking penumbra/umbra dots (e.g., Sobotka & Puschmann 2009). For the sunspot's interior, there were reports of outflows from f-mode analysis (Gizon et al. 2000), inflows at the depth of 1.5 - 5 Mm (Zhao et al. 2001), and large scale inflows around active regions up to 10 Mm in depth from ring-diagram analysis (Haber et al. 2004). Based on all these observations, Gizon (2003) proposed a schematic flow structure of the sunspot, and Hindman et al. (2009) recently proposed a similar one. Both flow structures show outflows near the surface, and inflows below that, with transition depth of these opposite flows undetermined. Here, based on all previous results, as well as on the recent numerical simulation of Evershed flows (Kitiashvili et al. 2009), we also propose a schematic flow structure of a sunspot (Figure 13), slightly different from the plots of two previous studies, but essentially similar. However, it is also acknowledged that this flow structure is not consistent with what was recently found by Gizon et al. (2009) and recent numerical simulations by Rempel et al. (2009). Thus, further observational and theoretical studies are required to determine the subsurface dynamics of sunspots.

The high resolution subsurface wave-speed maps (Figure 2) and flow fields (Figure 8), present us an unprecedented opportunity to see the sunspot's subsurface structures and dynamics with many details. These results reveal the complexity of the subsurface perturbations and dynamics and their relationship with the sunspot structure. The subsurface image at the depth of 0 – 1.5 Mm

displays a larger wave-speed perturbation, presumably hotter in temperature, near the light bridge area than other areas inside the sunspot, where the wave-speed perturbations are largely negative. This is in agreement with the surface observations that light bridges are formed by upwelling of hot plasma (Katsukawa et al. 2007). We also see clear divergent flows from the light bridge in high resolution subsurface flow map at the same depth (Figure 8). This is consistent with the plasma upwelling that occurs in this area, but not in good agreement with the proper motion tracking results of this region (Louis et al. 2008).

It is also interesting to see quite a few divergent flow cells inside both the sunspot umbra and penumbra. The cells are bigger than granules and smaller than supergranules, and indicate the existence of a mesoscale convection inside the sunspot. The discovery of these motions is intriguing because they may be a signature of the downdraft vortex rings around magnetic flux bundles, as suggested by Parker (1992). The Parker’s conjecture was that the observed clustering of magnetic flux bundles in sunspot is at least in part a consequence of hydrodynamic attraction of the downdraft vortex rings. Thus, it is very important to continue the investigations of the subsurface dynamics of sunspots, both observationally by high resolution helioseismology and theoretically by realistic MHD simulations.

5.2. Analysis without Phase-Speed Filtering

As introduced in §1, the phase-speed filtering may introduce some errors in active regions due to the smaller oscillation amplitude in these areas (Rajaguru et al. 2006), and using ridge filtering may give different results as using phase-speed filtering in active regions (Braun & Birch 2008). All of these prompt us a reexamination of the use of phase-speed filtering and an evaluation of how phase-speed filtering alter measured acoustic travel times, in particular, inside active regions.

The *Hinode* high resolution observation has helped us to overcome an obstacle that acoustic travel times could hardly be measured in short distances inside active regions if phase-speed filtering was not applied. Our measured distance-dependent acoustic travel time differences relative to the solar quiet region obtained without using the phase-speed filtering, as shown in Figure 11, have evidently demonstrated that for short distances, the acoustic travel time is longer inside both sunspot umbra and penumbra than the quiet region, and for distances longer than ~ 13 Mm, the mean travel time is shorter. This is generally in agreement with the measurements using phase-speed filters, except that the ones with filters would underestimate the values by 20–40% in sunspot umbra. It is believed that the underestimation is caused by a combination of oscillation amplitude suppression inside active regions and the use of phase-speed filtering. Therefore, we believe that the phase-speed filtering does not change qualitatively the measured travel times, therefore the inferred interior properties of active regions, but would change the inferred values quantitatively.

The *Hinode* data also enable us to construct acoustic travel time maps without using filters, and this gives us an opportunity to assess the correctness and accuracy of various filters. Further investigations are particularly important in this regard.

5.3. Summary

We summarize our results as follows:

1. By analyzing high resolution *Hinode* Ca II H observations using time-distance helioseismology, we have derived wave-speed structures beneath solar active regions. The inferred structures are remarkably similar to results obtained by various authors analyzing MDI Dopplergram observations, although the instrument, the spectrum line used to observe, the type of observation (intensity and Doppler velocity), the inversion technique, and the sensitivity kernels are mostly different.
2. The subsurface flow field structure is generally in agreement with previous MDI result, but it is clear that the downward flows near the sunspot surface is more prominent, and the mass circulation around the sunspot is more clear and seems self-consistent, although no mass conservation constraint is applied in the inversion.
3. Our analysis without using phase-speed filtering has convincingly demonstrated that the phase-speed filtering does not change travel time measurements qualitatively, but may underestimate travel time anomalies inside active regions.
4. High spatial resolution subsurface flow fields reveal quite a few organized flow structures inside sunspot umbra and penumbra, which are perhaps corresponding to some convection structures or downdraft vortex rings around magnetic flux bundles. In the light bridge area, subsurface hotter temperature is found, and plasma flows divergent from the light bridge is also seen. These initial results provide a basis for further development of high-resolution acoustic tomography of sunspots, and comparison with numerical simulations.

We thank Dr. I. Kitiashvili for making Fig. 13 for us. We also appreciate an anonymous referee for raising a few important questions that helped to improve the quality of this paper. *Hinode* is a Japanese mission developed and launched by ISAS/JAXA, collaborating with NAOJ as a domestic partner, NASA and STFC (UK) as international partners. Scientific operation of the *Hinode* mission is conducted by the *Hinode* science team organized at ISAS/JAXA. This team mainly consists of scientists from institutes in the partner countries. Support for the post-launch

operation is provided by JAXA and NAOJ (Japan), STFC (U.K.), NASA, ESA, and NSC (Norway). This work was (partly) carried out at the NAOJ *Hinode* Science Center, which is supported by the Grant-in-Aid for Creative Scientific Research “The Basic Study of Space Weather Prediction” from MEXT, Japan (Head Investigator: K. Shibata), generous donations from Sun Microsystems, and NAOJ internal funding.

REFERENCES

- Basu, S., Antia, H. M., & Bogart, R. S. 2004, *ApJ*, 610, 1157
- Bogart, R. S., Basu, S., Rabello-Soares, M. C., & Antia, H. M. 2008, *Sol. Phys.*, 251, 439
- Braun, D. C., & Birch, A. C. 2008, *Sol. Phys.*, 251, 267
- Cally, P. S. 2009, *Sol. Phys.*, 254, 241
- Carlsson, M., et al. 2007, *PASJ*, 59, S663
- Couvidat, S., Birch, A.C., & Kosovichev, A. G. 2006, *ApJ*, 640, 516
- Couvidat, S., Birch, A. C., Kosovichev, A. G., & Zhao, J. 2004, *ApJ*, 607, 554
- Duvall, T. L., Jr., D’Silva, S., Jefferies, S. M., Harvey, J. W., & Schou, J. 1996, *Nature*, 379, 235
- Duvall, T. L., Jr., et al. 1997, *Sol. Phys.*, 170, 63
- Gizon, L., Ph.D. Thesis, Chapter. 5.1, 2003, Stanford Univ.
- Gizon, L., Duvall, T. L., Jr., & Larsen, R. M. 2000, *J. Astrophys. Astron.*, 21, 339
- Gizon, L., et al. 2009, *Space Science Reviews*, 144, 249
- Haber, D. A., Hindman, B. W., Toomre, J., & Thompson, M. J. 2004, *Sol. Phys.*, 220, 371
- Hindman, B. W., Gizon, L., Duvall, T. L., Jr., Haber, D. A., & Toomre, J. 2004, *ApJ*, 613, 1253
- Hindman, B. W., Haber, D. A., & Toomre, J. 2009, *ApJ*, 698, 1749
- Hurlburt, N., & DeRosa, M. 2008, *ApJ*, 684, L123
- Hurlburt, N. E., & Rucklidge, A. M. 2000, *MNRAS*, 314, 793
- Jensen, J. M., Duvall, T. L., Jr., Jacobsen, B. H., & Christensen-Dalsgaard, J. 2001, *ApJ*, 553, L193

- Katsukawa, Y., et al. 2007, PASJ, 59, S577
- Kitiashvili, I. N., Kosovichev, A. G., Wray, A. A., & Mansour, N. N. 2009, ApJ, 700, L178
- Komm, R., Howe, R., Hill, F., González Hernández, I., Toner, C., & Corbard, T. 2005, ApJ, 631, 636
- Kosovichev, A. G. 1996, ApJ, 461, L55
- Kosovichev, A. G., & Duvall, T. L., Jr. 1996, in *Proceedings of SCORE'96 Workshop: Solar Convection and Oscillations and Their Relationship*, ed. F. P. Pijpers, J. Christensen-Dalsgaard & C. S. Rosenthal (Dordrecht: Kluwer), 241
- Kosovichev, A. G., Duvall, T. L., Jr., & Scherrer, P. H. 2000, Sol. Phys., 192, 159
- Kosugi, T., et al. 2007, Sol. Phys., 243, 3
- Lindsey, C., & Braun, D. C. 2005a, ApJ, 620, 1107
- Lindsey, C., & Braun, D. C. 2005b, ApJ, 620, 1118
- Louis, R. E., Bayanna, A. R., Mathew, S. K., & Venkatakrisnan, P. 2008, Sol. Phys., 252, 43
- Nagashima, K., Sekii, T., Kosovichev, A. G., Zhao, J., & Tarbell, T. D. 2009, ApJ, 694, L115
- Parchevsky, K. V., Zhao, J., & Kosovichev, A. G. 2008, ApJ, 678, 1498
- Parker, E. N. 1979, ApJ, 230, 905
- Parker, E. N. 1992, ApJ, 390, 290
- Rajaguru, S. P., Birch, A. C., Duvall, T. L., Jr., Thompson, M. J., & Zhao, J. 2006, ApJ, 646, 543
- Rempel, M., Schüssler, M., Cameron, R. H., & Knölker, M. 2009, Science, 325, 171
- Scherrer, P. H., et al. 1995, Sol. Phys., 162, 129
- Schunker, H., Braun, D. C., Cally, P. S., & Lindsey, C. 2005, ApJ, 621, L149
- Sekii, T., et al. 2007, PASJ, 59, S637
- Sobotka, M., & Puschmann, K. G. 2009, A&A, 504, 575
- Tsuneta, S., et al. 2008, Sol. Phys., 249, 167

Zhao, J., Georgobiani, D., Kosovichev, A. G., Bensen, D., Stein, R. F., & Nordlund, Å. 2007, *ApJ*, 659, 848

Zhao, J., & Kosovichev, A. G. 2003a, in *Proceeding of SOHO 12/ GONG+ 2002 Workshop, Local and Global Helioseismology: the Present and Future*, ed. H. Sawaya-Lacoste (ESA SP-517; Noordwijk: ESA), 417

Zhao, J., & Kosovichev, A. G. 2006, *ApJ*, 643, 1317

Zhao, J., Kosovichev, A. G., & Duvall, T. L., Jr. 2001, *ApJ*, 557, 384

Zharkov, S., Nicholas, C. J., & Thompson, M. J. 2007, *Astron Nachr*, 328, 240

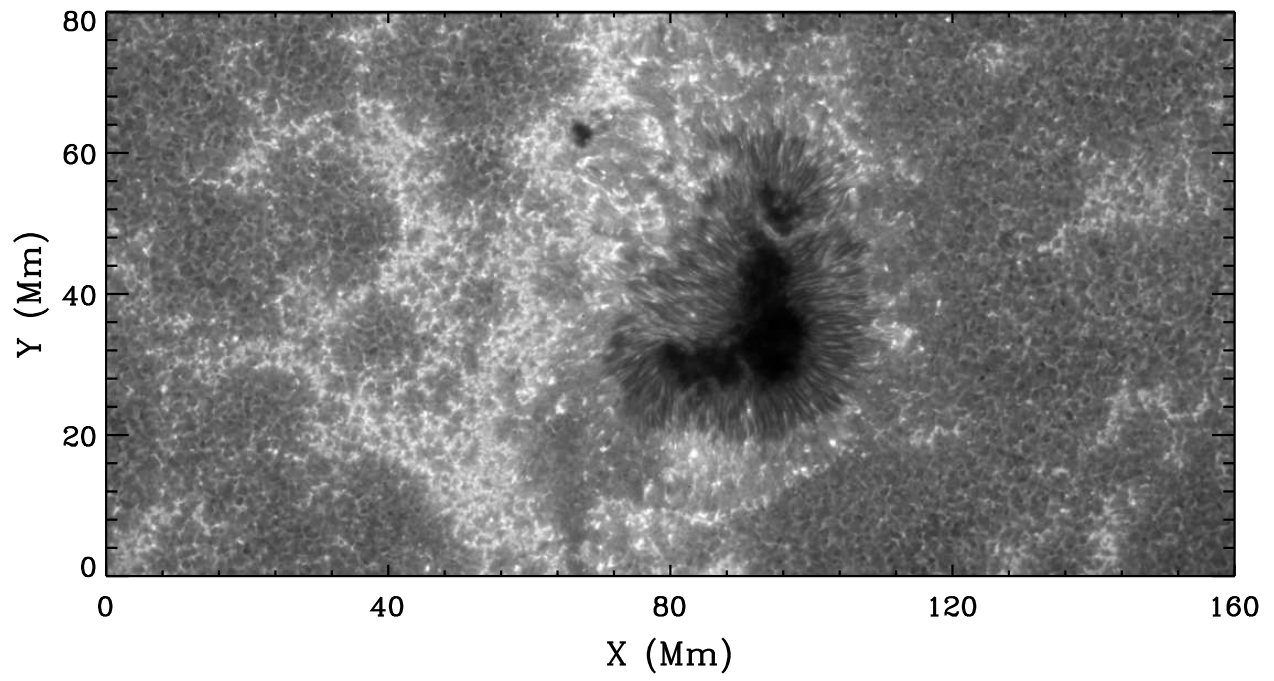


Fig. 1.— A Ca II H image of the studied region from the *Hinode*/SOT.

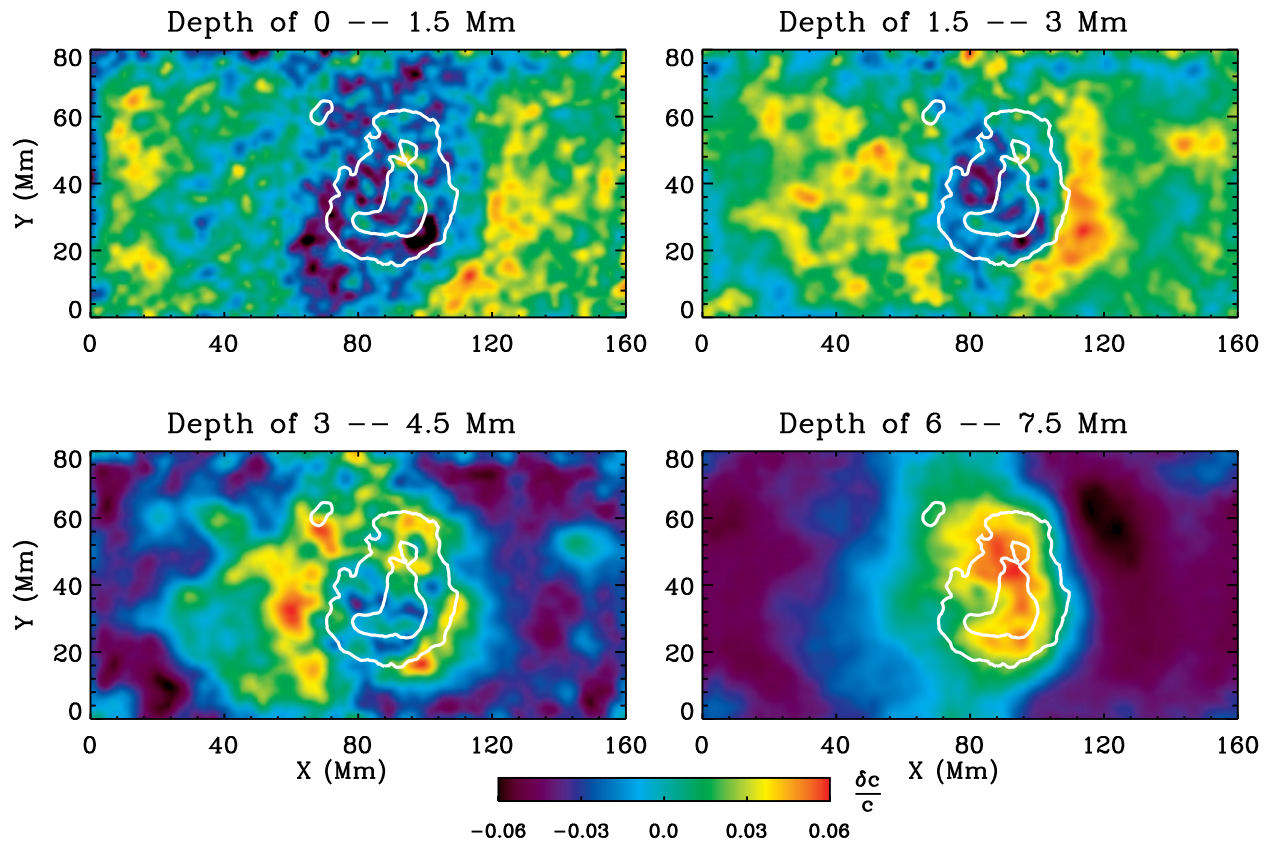


Fig. 2.— Sound speed perturbation at different depths. The white contours in each panel indicate the boundaries of sunspot umbra and penumbra.

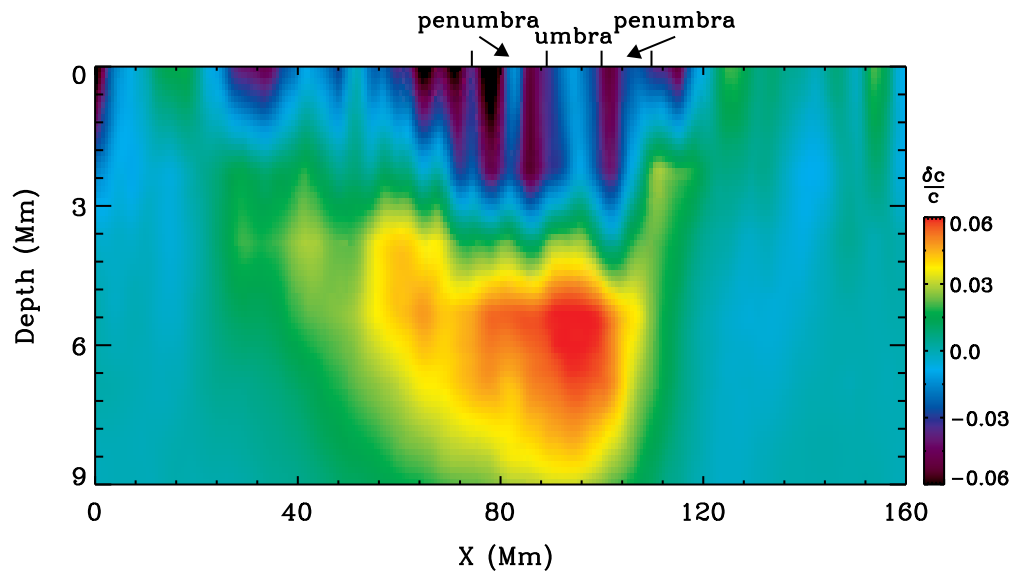


Fig. 3.— A vertical view of sound speed perturbation beneath the active region.

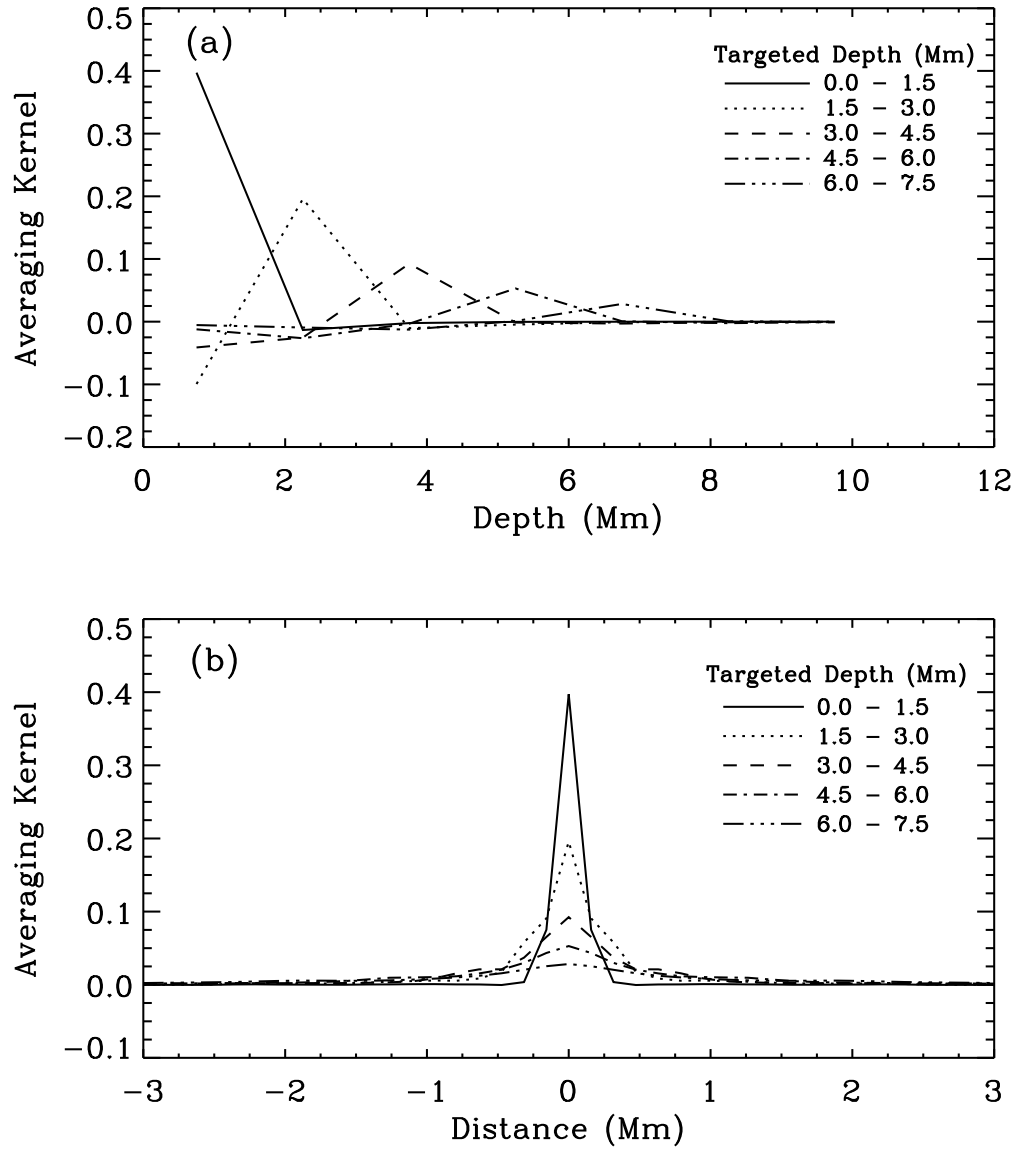


Fig. 4.— Averaging kernels, as functions of (a) depth and (b) horizontal distance, for different targeted depths obtained from acoustic wave speed perturbation inversion.

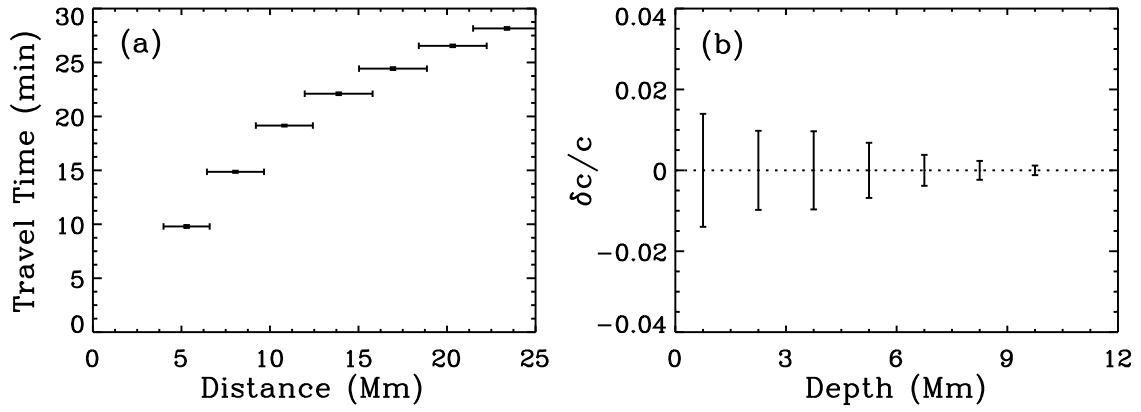


Fig. 5.— (a) Measured mean travel times obtained in a piece of quiet Sun. Horizontal error bars indicate the measurement annulus ranges, and vertical error bars indicate standard deviations from this area. (b) Error estimates from acoustic wave speed perturbations at each targeted depth.

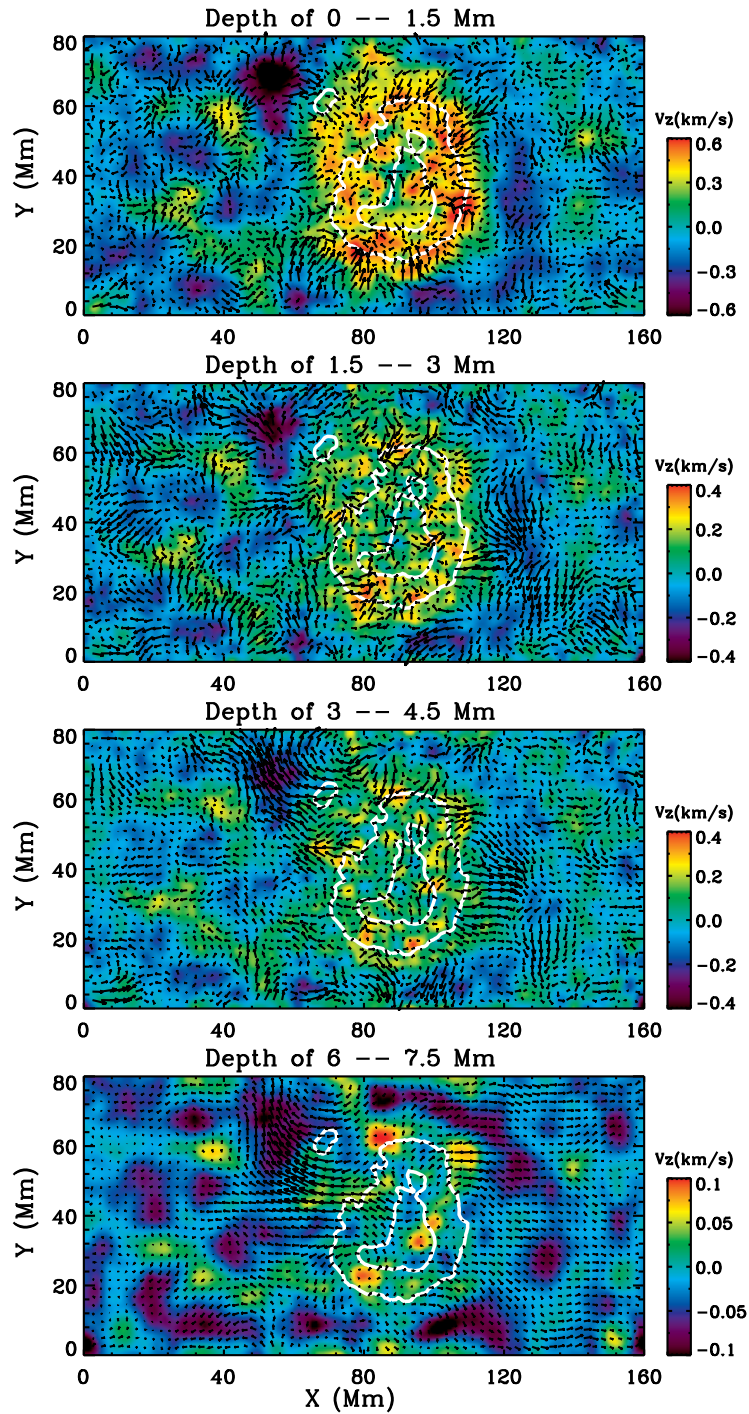


Fig. 6.— Subsurface flow fields at different depths. Background images indicate vertical flow fields, with positive representing downflows and negative as upflows. Arrows indicate horizontal flows, with the longest arrow representing a velocity of approximately 500 m/s in each panel. White contours in each panel display the boundaries of sunspot umbra and penumbra.

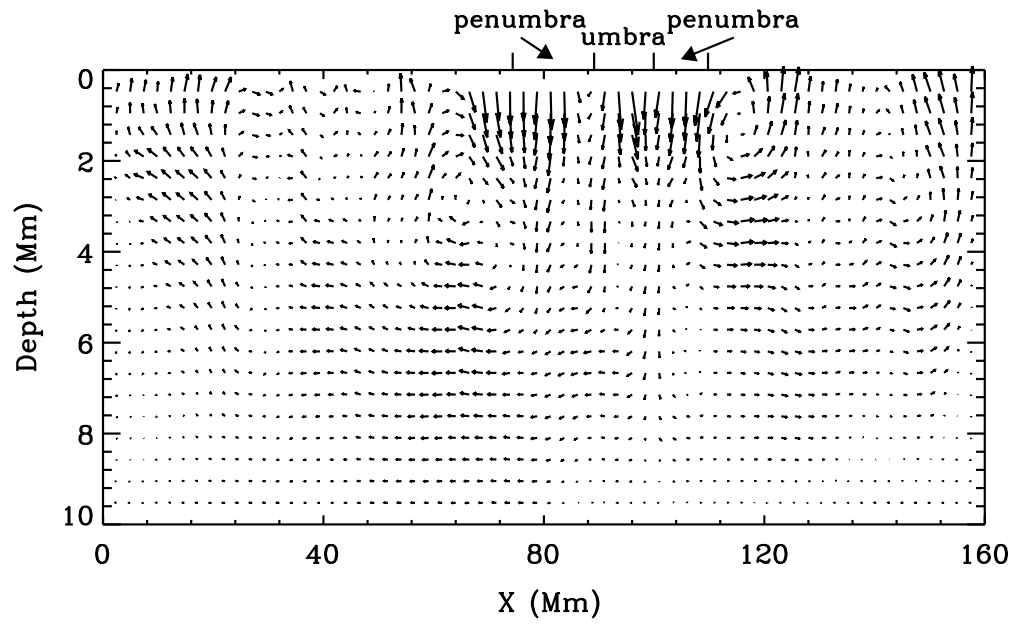


Fig. 7.— A vertical view of flow field beneath the active region. The longest arrow is approximately 500 m/s.

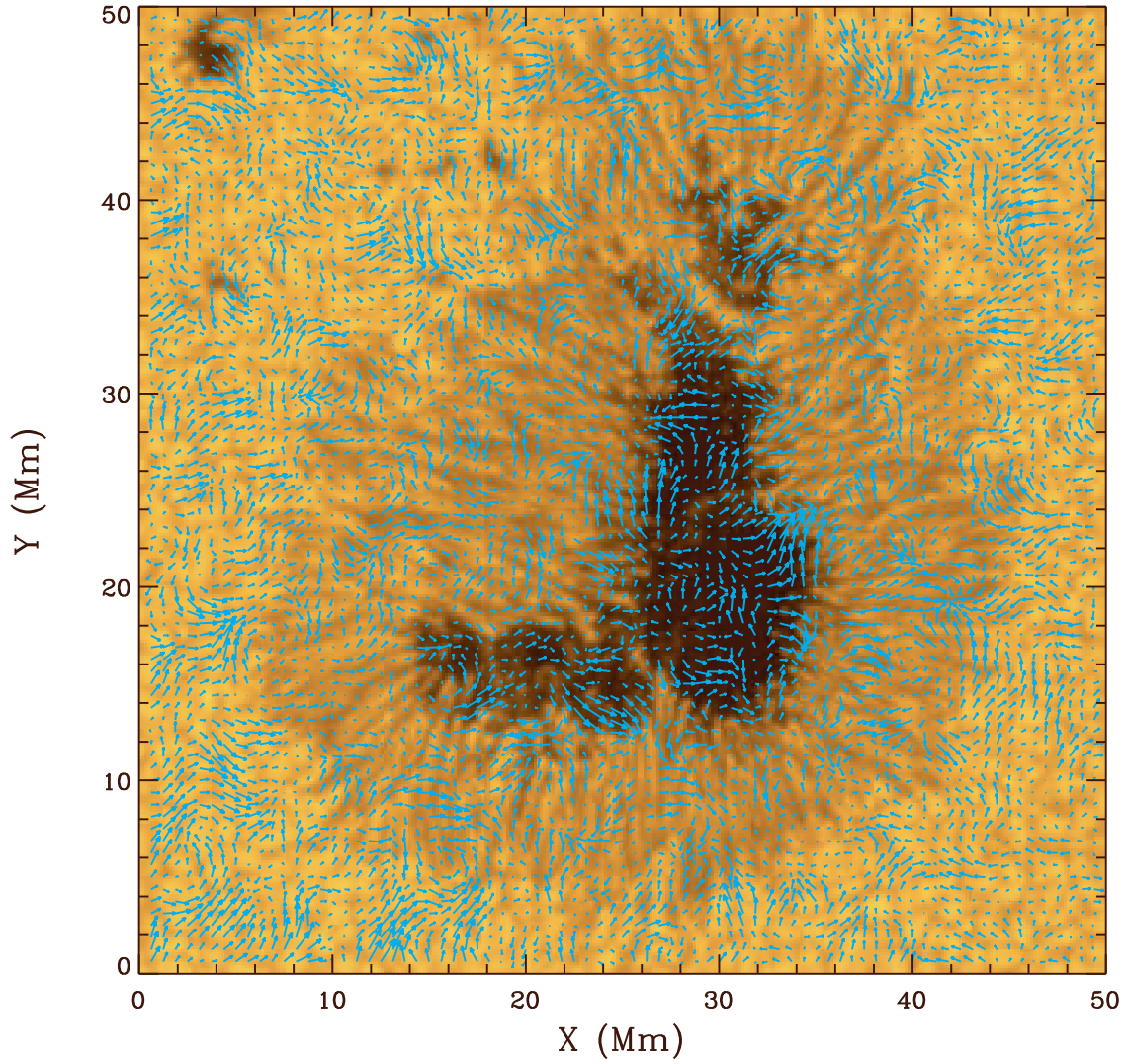


Fig. 8.— High resolution horizontal flow field 0 - 1.5 Mm beneath the sunspot region. The background image is this sunspot observed at the photospheric level. The longest arrow indicates a speed of 800 m/s.

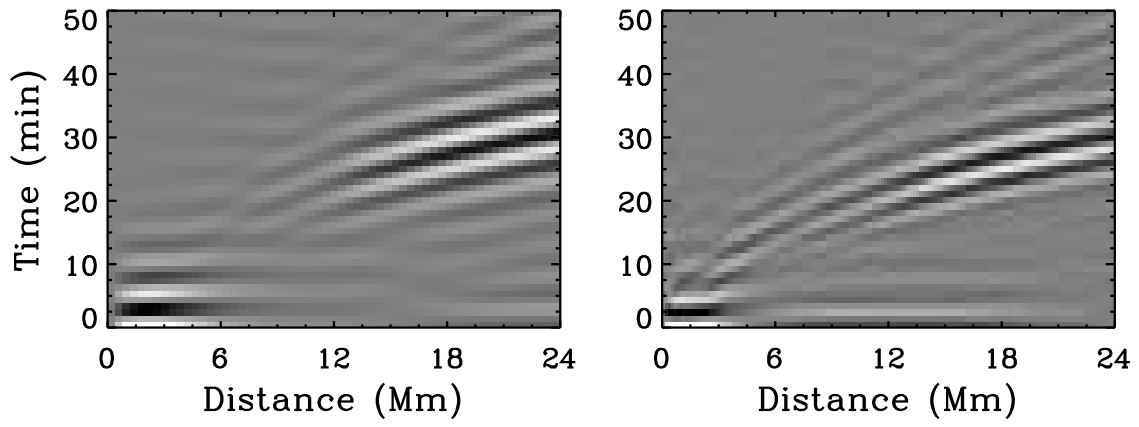


Fig. 9.— Time-distance diagrams obtained from MDI high-resolution Dopplergram (*left*) and *Hinode* (*right*) Ca II H observations.

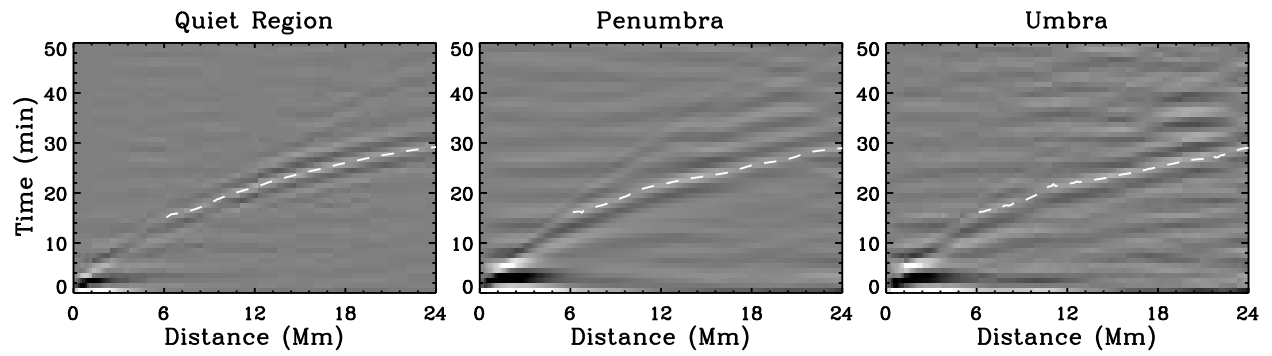


Fig. 10.— Time-distance diagrams obtained when the central points are located inside a quiet region, sunspot penumbra, and sunspot umbra, respectively. The dashed line in each panel is the travel times fitted from the corresponding time-distance diagram.

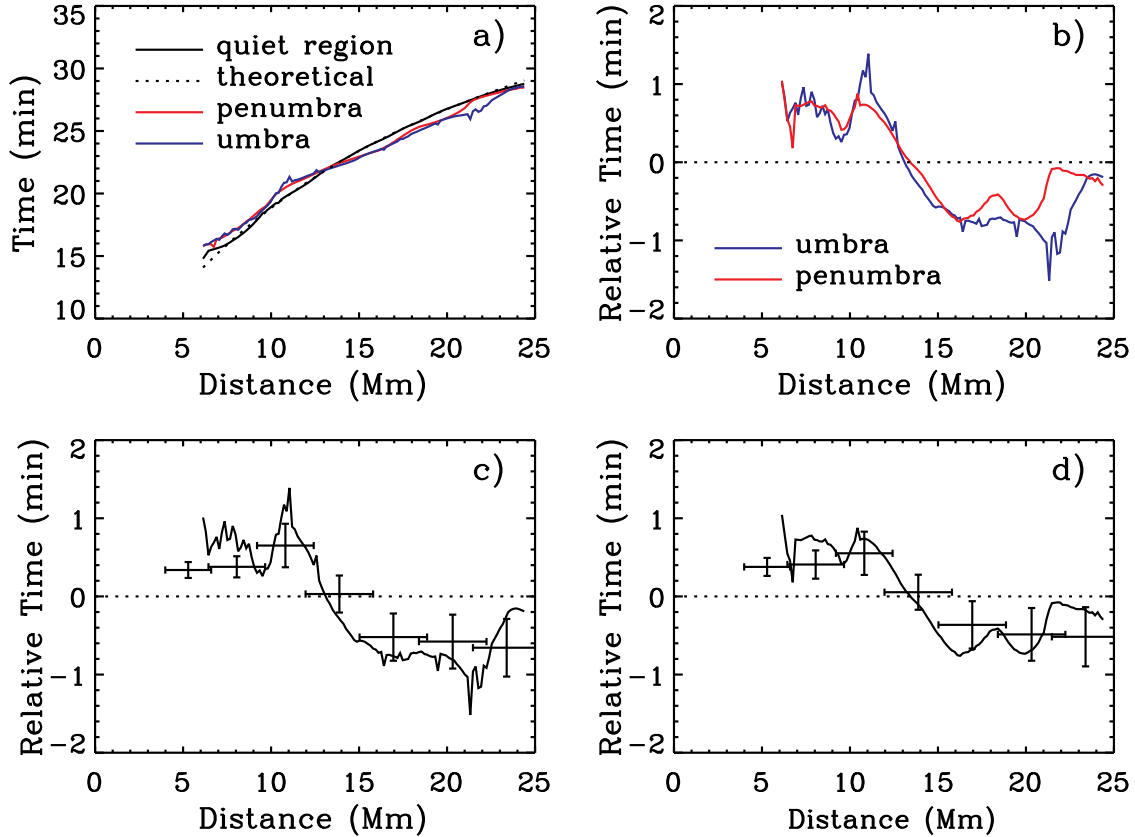


Fig. 11.— a) Comparison of travel times obtained in solar quiet region, sunspot penumbra, and sunspot umbra. Solid lines are the same as dashed lines in Figure 10, and the dotted line is a theoretical expectation of travel times from ray theory. b) Travel time differences relative to the quiet region for sunspot penumbra and umbra. c) Comparison of travel time differences with and without using phase-speed filtering. Solid line is the same as the umbra line in b), and the points with error bars are mean travel times averaged from the travel time maps obtained with the use of phase-speed filtering (i.e., measurements used in §3), but only points inside sunspot umbra are used for average. Horizontal error bars indicate the annulus radius range, and the vertical error bars indicate the standard errors. d) Same as panel c), but solid lines and points with error bars are both obtained inside sunspot penumbra.

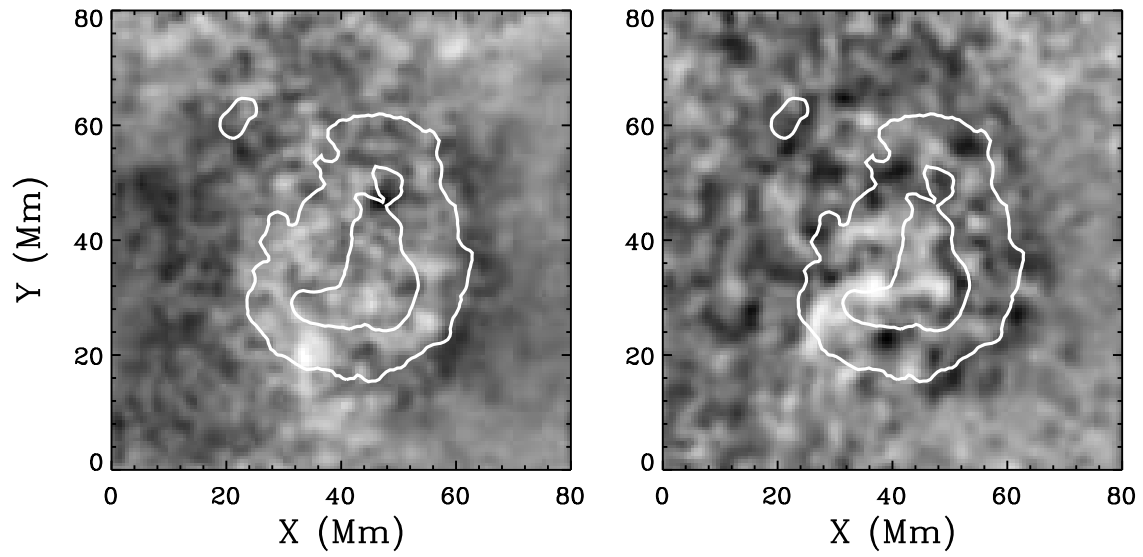


Fig. 12.— Comparison of mean travel time maps obtained with (*left*) and without (*right*) the phase-speed filtering. The annulus radius range is 12.0 – 15.9 Mm, same for both measurements. White contours indicate the boundaries of sunspot umbra and penumbra.

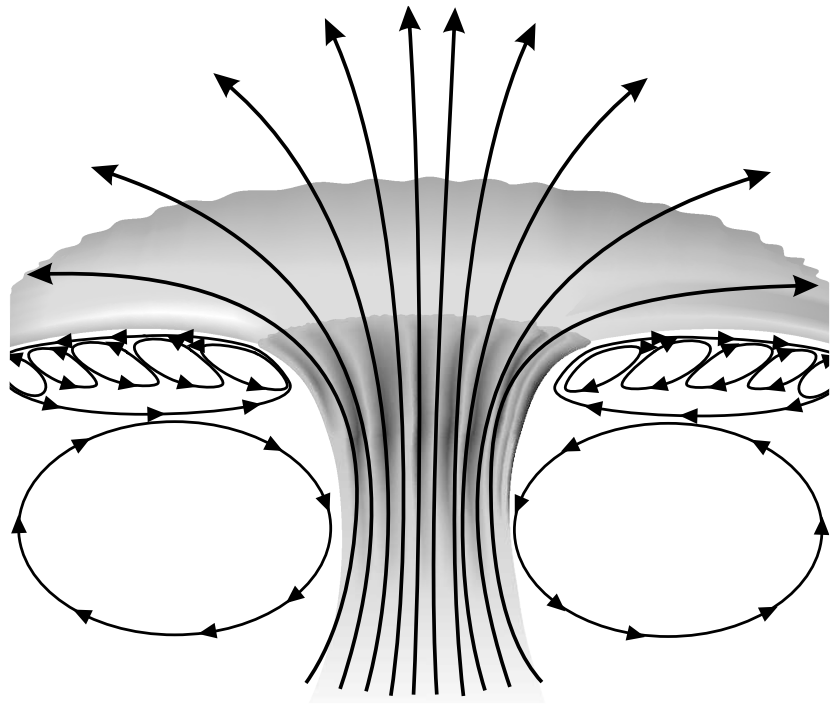


Fig. 13.— A schematic plot of sunspot's flow structure near the surface and in the interior.